Supplementary Information (SI) for Nanoscale Horizons.
This journal is © The Royal Society of Chemistry 2024

Supplementary Material for Processes to enable the hysteresis-free operation of ultrathin ALD Te p channel field-effect transistors

*Minjae Kim [a], Yongsu Lee [b], Kyuheon Kim [a], Giang-Hoang Pham [c], Kiyung Kim [a], Jae Hyeon Jun [a], Hae-won Lee [a], Seongbeen Yoon [a], Hyeon Jun Hwang [d], Myung Mo Sung [c] and Byoung Hun Lee *[a]*

[a.] *Department of Electrical Engineering, Pohang University of Science and Technology (POSTECH), 77, Cheongam–ro, Nam–gu, Pohang–si, Gyeongsangbuk–do 37673, Republic of Korea. E–mail: bhlee1@postech.ac.kr*

[b.] *Advanced Radiation Technology Institute, Korea Atomic Energy Research Institute,29 Geumgu-gil, Jeongeup-si, Jeolabuk-do, 56212 Republic of Korea*

[c.] *Department of Chemistry, Hanyang University, Wangsimni-ro 222, Seongdong-gu Seoul 04763, Republic of Korea*

[d.] *Department of Semiconductor Engineering, Mokpo National University, 1666, Yeongsan–ro, Cheonggye–myeon, Muan–gun, Jeollanam–do 58554, Republic of Korea.*

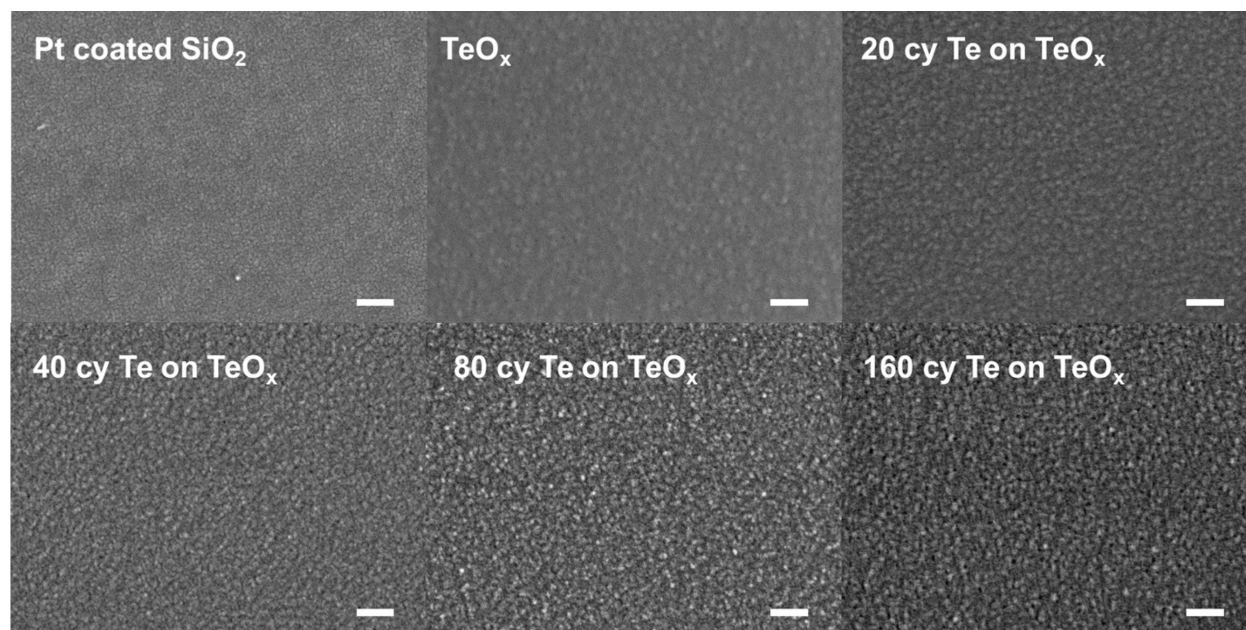

Figure S1. SEM images of surfaces with varying Te ALD cycles. Scale bar: 100 nm. The distinct Te grains observed after multiple ALD cycles indicate the contribution of the TeO_x seed layer.

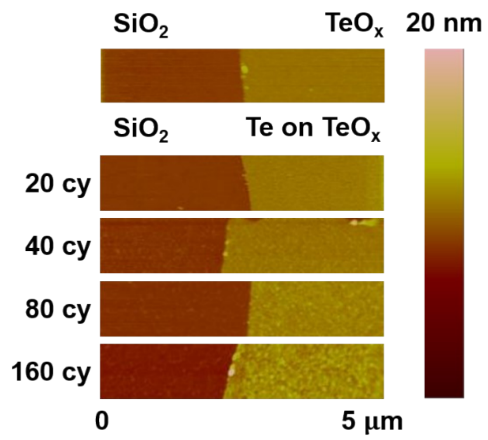

Figure S2. AFM images of surfaces with varying Te ALD cycles.

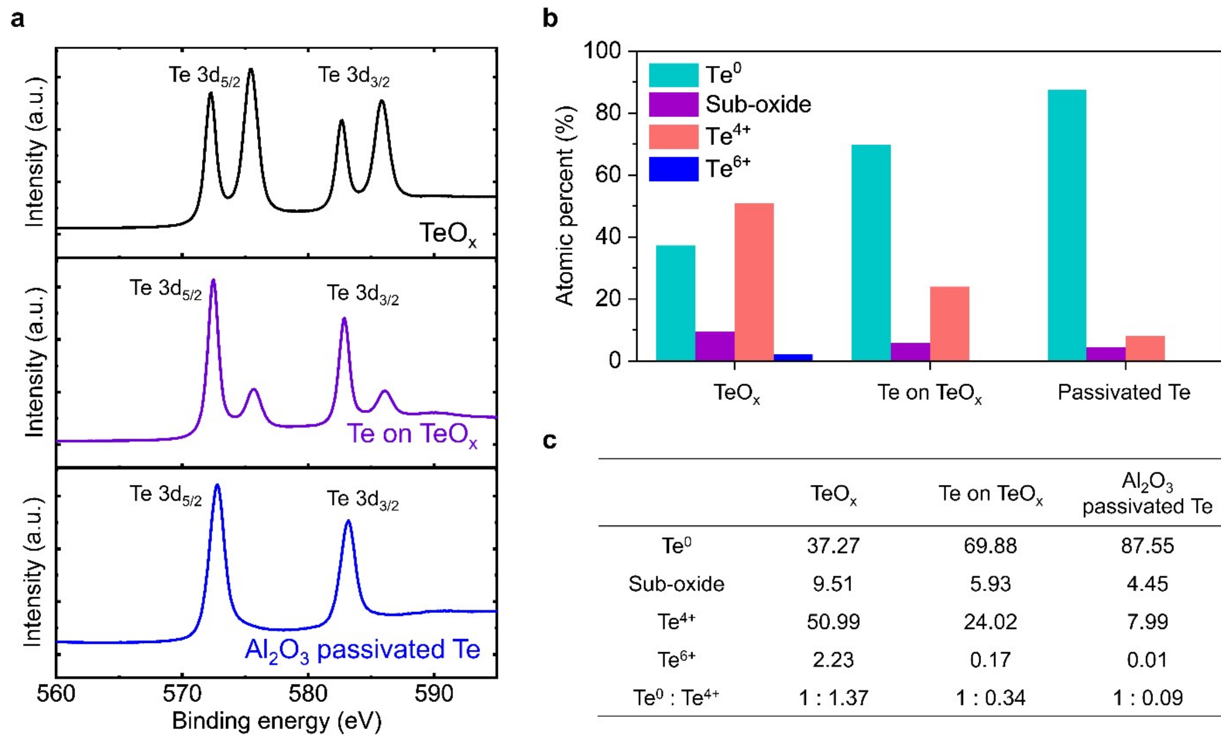

	TeO_x	Te on TeO_x	Al_2O_3 passivated Te
Te^0	37.27	69.88	87.55
Sub-oxide	9.51	5.93	4.45
Te^{4+}	50.99	24.02	7.99
Te^{6+}	2.23	0.17	0.01
Te^0 : Te^{4+}	1 : 1.37	1 : 0.34	1 : 0.09

Figure S3. XPS spectra and atomic composition analysis. (a) XPS spectra of Te 3d peak of the TeO_x layer (top), Te/TeO_x layer (middle), and Al_2O_3 passivation layer/Te/TeO_x layer (bottom). Atomic compositions were extracted from the deconvoluted Te $3d_{5/2}$ peak. (b) Column graph and (c) atomic composition analysis.

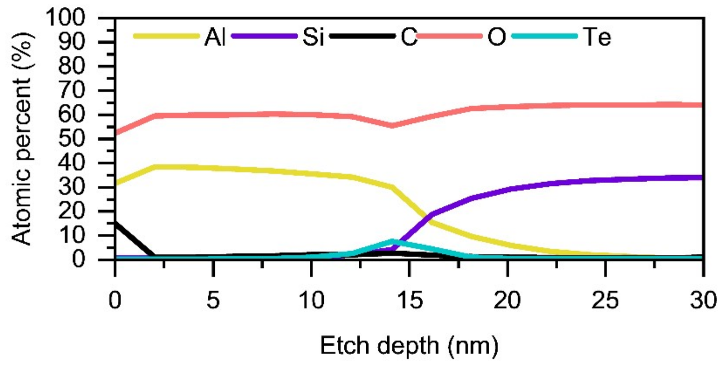

Figure S4. XPS depth profile analysis. Depth profile result of Al_2O_3 passivated Te on the SiO_2/Si substrate.

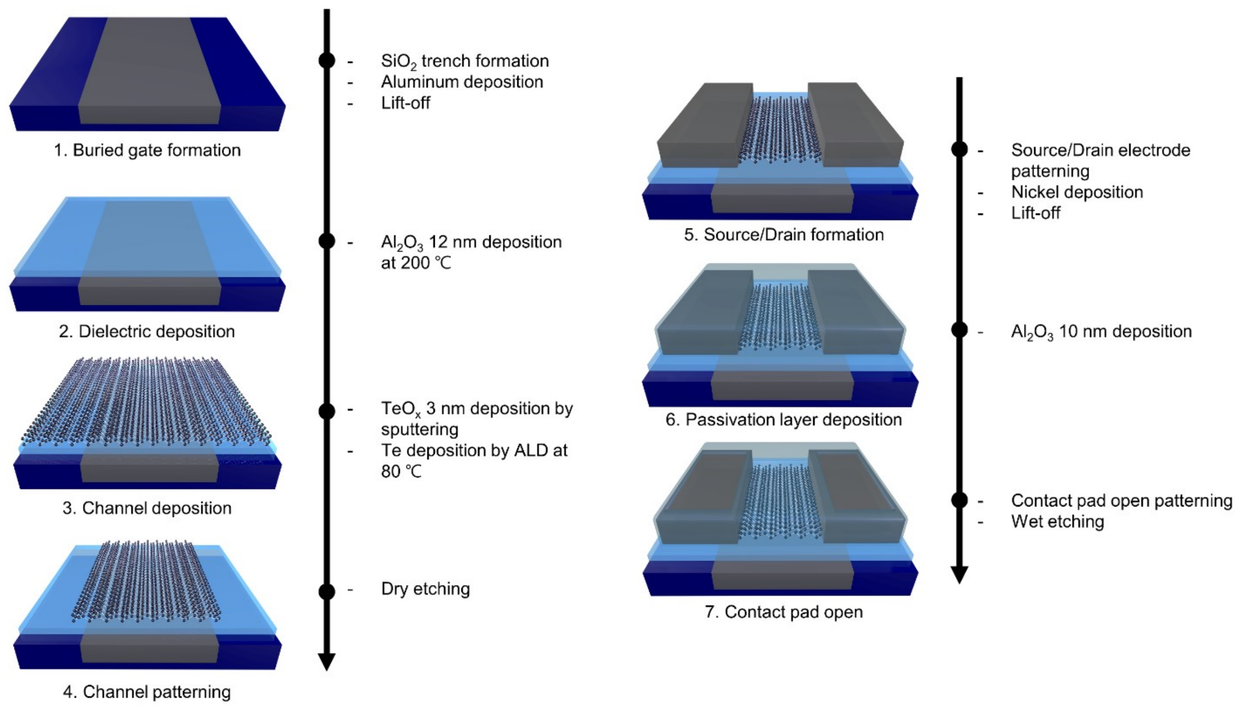

Figure S5. Schematic of the fabrication process of Te pFET.

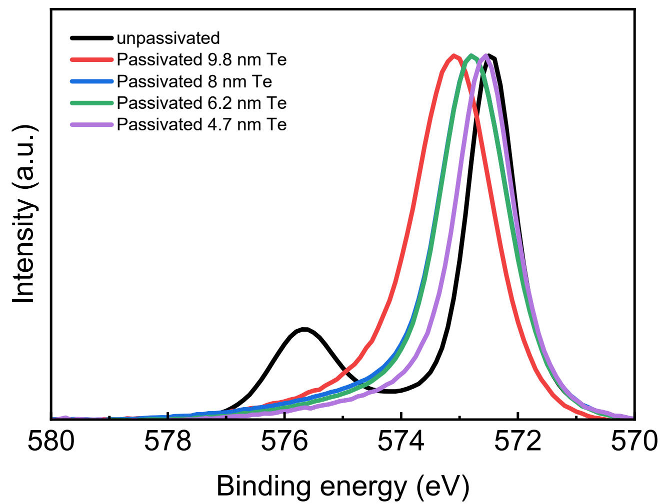

Figure S6. XPS spectra before and after passivation with varying Te thickness. As the thickness of tellurium decreases, the Te^0 peak shifts to 572.5 eV and the peak width narrows, indicating a reduction in the oxide-related peak.

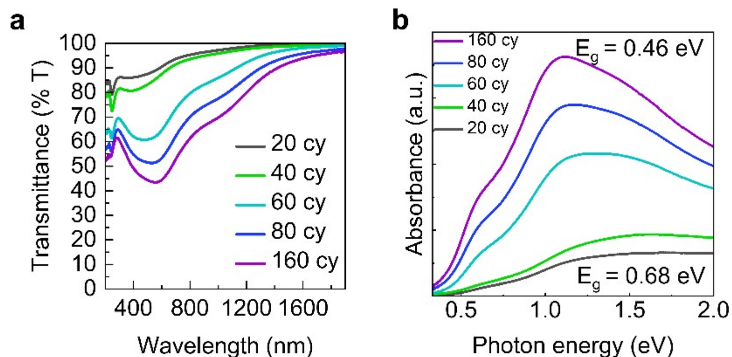

Figure S7. Optical characteristics of Te films with varying thicknesses as measured by UV-Vis spectroscopy. a, UV-vis transmittance spectra, **b**, Absorption spectra with optical bandgap.

The transmission and absorption spectra measured using UV-visible spectroscopy (wavelength range of 380–700 nm) show that the average transmittance decreased from 90.8% to 48.5% as the number of ALD cycles increases (Figure S7a). The optical bandgap of Te is extracted from its absorption spectrum, as shown in Figure S7b. As expected, the optical bandgap is higher for a thinner Te—0.68 eV for 20 cycles and 0.46 eV for the 160 cycle Te.

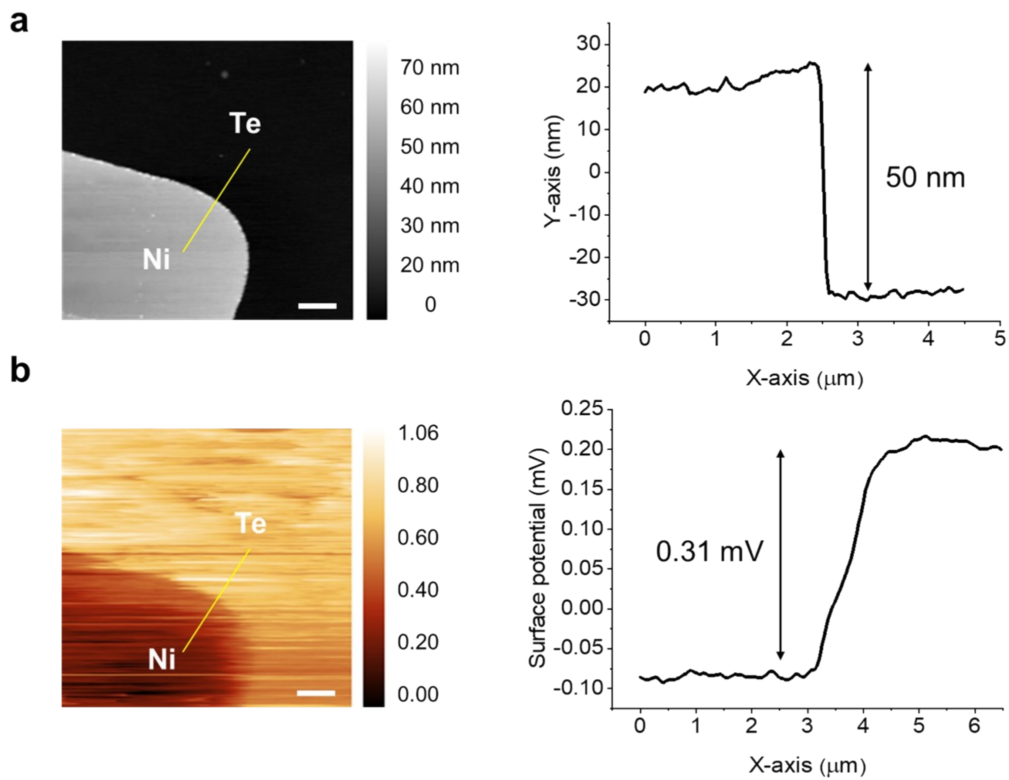

Figure S8. KPFM data of the Ni/Te boundary. (a) Surface topology image and thickness profile. (b) Surface potential map and potential profile. All scale bars: 1 μm.

Using KPFM measurements, the surface potential difference between the tip and the measured materials can be determined. Using the measured potential difference, the Fermi level difference between Ni and Te was extracted.

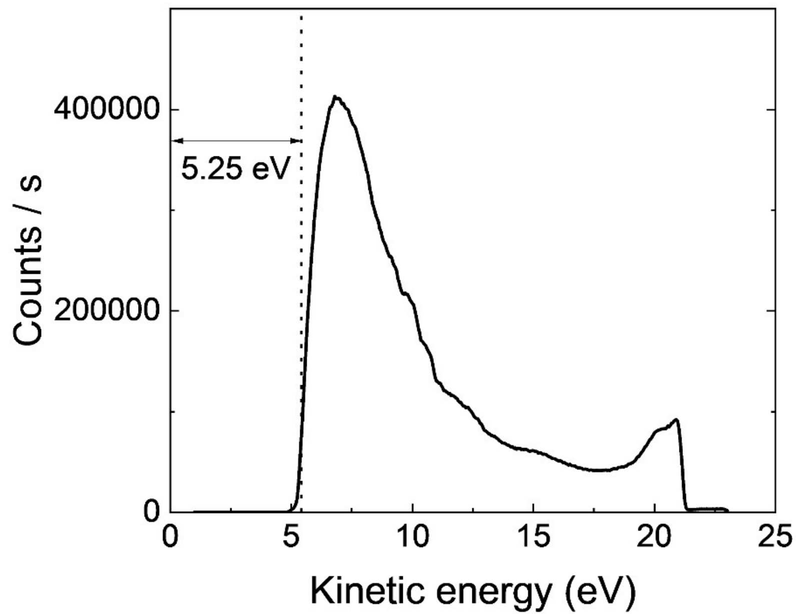

Figure S9. Ni work function extraction from UPS. The extracted work function is approximately 5.25 eV.

To determine the work function of Ni electrode, UPS measurements were conducted. The measured work function of Ni was 5.25 eV, which is consistent with values reported in previous literature1. Using the work function of Ni and surface potential data, an ideal band diagram is proposed.

References

1 S. C. Lim, J. H. Jang, D. J. Bae, G. H. Han, S. Lee, I.-S. Yeo and Y. H. Lee, *Appl. Phys. Lett.*, 2009, 95.